Acenaphtho[1,2-*d*][1,2,3]triazole and Its Kuratowski Complex: A π-Extended Tecton for Supramolecular and Coordinative Self-Assembly

Katharina Knippen[+],[a] Daniel Matuszczyk[+],[b] Maryana Kraft,[a] Björn Bredenkötter,[a] Georg Eickerling,[c] Tadeusz Lis,[b] Dirk Volkmer,*[a] and Marcin Stępień*[b]

Abstract: π-Extended acenaphtho[1,2-*d*][1,2,3]triazoles, the unsubstituted Anta-H and its di-*tert*-butyl derivative Diban-ta-H, as well as 5,6,7,8-tetrahydro-1*H*-naphtho[2,3-*d*][1,2,3]triazole Cybta-H were obtained in concise syntheses. In the solid state, Dibanta-H forms an unprecedented hydrogen-bonded cyclic tetrad, stabilized by dispersion interactions of the bulky *t*Bu substituents, whereas a cyclic triad was found in the crystal structure of Anta-H. These cyclic assemblies form infinite slipped stacks in the crystals. Evidence for analogous hydrogen-bonded self-assembly in solution was provided by low-temperature NMR spectroscopy and computational analyses. Kuratowski-type pentanuclear complexes $[Zn_5Cl_4(Dibanta)_6]$ and $[Zn_5Cl_4(Cybta)_6]$ were prepared from the respective triazoles. In the Dibanta complexes, the π-aromatic surfaces of the ligands extend from the edges of the tetrahedral Zn_5 core, yielding an enlarged structure with significant internal molecular free volume and red-shifted fluorescence.

π-Extended heterocyclic building blocks are of great interest as the structural components of functional organic dyes and coordination compounds.[1] By fusing a reactive heterocyclic ring with a larger aromatic framework, it is possible to obtain tunable motifs that can be combined into larger chromophores and act as ligands in molecular complexes as well as in framework materials. π-Extension of pyrroles, for instance, has been intensely explored as a general strategy toward low-bandgap porphyrinoids and other oligopyrrolic molecules.[1,2] In this context, fusion of acenaphthylene to the β-β edge of pyrrole (**1**–**2**, Figure 1) provided particularly striking examples of π-extended chromophores,[3,4] and has been more recently elaborated into a general strategy toward oligopyrrole-naphthalenemonoimide hybrids,[4–10] characterized by extended NIR absorptions and multilevel redox chemistry. Acenaphthylene-fused imidazoles (**3**) have found use as precursors of N-heterocyclic ligands with applications in Pd-, Ni-, and Cu-catalyzed coupling reactions.[11–14]

Inspired by these advances, we considered acenaphthylene fusion as a means of creating π-extended 1,2,3-triazoles. The target system, acenaphtho[1,2-*d*][1,2,3]triazole (**4**, Figure 1) was envisaged as an enlarged ligand for pentanuclear Kuratowski-type complexes $[M^{II}_5X_4(triazolate)_6]$,[15–17] so named because of their formal relationship to K. Kuratowski's $K_{3,3}$ graph.[18,19] These complexes have been used as secondary building units (SBUs) in a range of metal–organic frameworks (MOFs),[20–25] including systems containing bis-triazole ligands, such as MFU-4,[22] CFA-1,[23] CFA-7,[24] and CFA-8.[25] Here we show that, in spite of its enlarged aromatic core, triazole **4** can be fitted into Kuratowski-

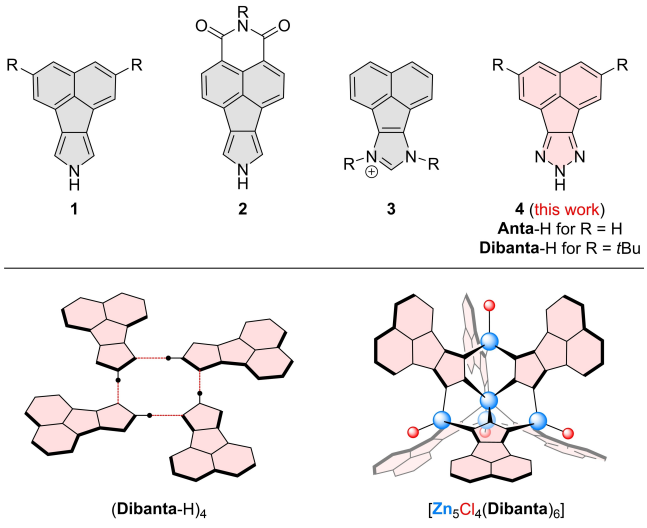

Figure 1. Acenaphthylene-fused heterocycles (top) and architectures based on Dibanta-H (bottom, this work).

[a] *K. Knippen,[+] Dr. M. Kraft, Dr. B. Bredenkötter, Prof. Dr. D. Volkmer*
Institute of Physics, Chair of Solid State and Materials Science
Augsburg University
Universitätsstrasse 1, 86159 Augsburg (Germany)
E-mail: dirk.volkmer@physik.uni-augsburg.de

[b] *D. Matuszczyk,[+] Prof. T. Lis, Prof. M. Stępień*
Wydział Chemii
Uniwersytet Wrocławski
ul. F. Joliot-Curie 14, 50-383 Wrocław (Poland)
E-mail: marcin.stepien@chem.uni.wroc.pl

[c] *Dr. G. Eickerling*
Institute of Physics, Chair of Chemical Physics and Materials Science
Augsburg University
Universitätsstrasse 1, 86159 Augsburg (Germany)

[+] *These authors contributed equally to this work.*

Supporting information for this article is available on the WWW under https://doi.org/10.1002/chem.202103480

type structures yielding fluorescent complexes characterized by moderate porosity in the solid state. In addition, the free triazole possesses an ability to self-assemble into unprecedented quadruplex structures stabilized by a combination of hydrogen bonding and dispersive interactions.

8*H*-Acenaphtho[1,2-*d*][1,2,3]triazole (Anta-H) and 2,5-di-*tert*-butylacenaphtho[1,2-*d*][1,2,3]triazole (Dibanta-H) were obtained from acenaphthylene **5a**[26] and 2,7-di-*tert*-butylacenaphthylene **5b**,[27] respectively, in a two-step synthesis (Scheme 1). First, **5a** and **5b** were converted to their *p*-toluene sulfonyl derivatives, **6a** and **b**, using the iodosulfonation/elimination sequence. In the second step, the sulfones were annulated with sodium azide to provide the desired fused 1,2,3-triazoles Anta-H and Dibanta-H in a 93% and 44% yield, respectively. A reference ligand, 5,6,7,8-tetrahydro-1*H*-naphtho[2,3-*d*][1,2,3]triazole (Cybta-H) was prepared by Pd-catalyzed hydrogenation of 2,3-naphtalenediamine **7**, followed by reaction with sodium nitrite. Kuratowski-type complexes $[Zn_5Cl_4(Dibanta)_6]$, and $[Zn_5Cl_4(Cybta)_6]$, were obtained using slightly modified literature procedures,[28,29] by treating zinc chloride with the corresponding triazole ligand, in the presence of 2,6-lutidine as a base at room temperature, followed by recrystallization.

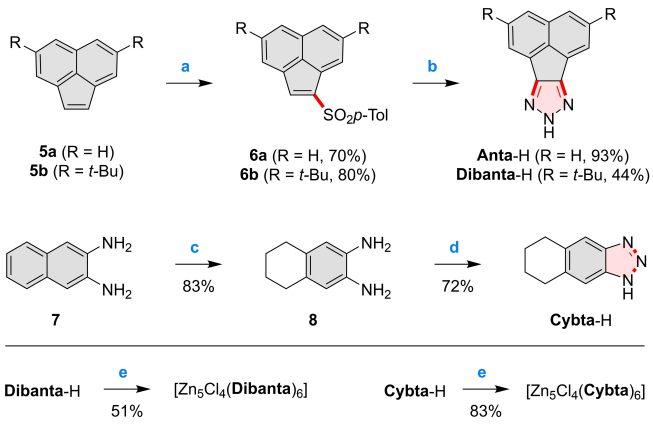

Scheme 1. Syntheses of triazoles and their Kuratowski complexes. a) i: *p*-TolSO_2Na, I_2, CH_2Cl_2/H_2O, RT, 24 h; ii: DBU, PhMe, RT, 1 h; b) NaN_3, DMF, 120 °C, 24 h; c) Pd/C, 60 bar H_2, RT, 5 days; d) $NaNO_2$, 5 °C, 2 h; e) $ZnCl_2$, DMF, RT, 2 days.

Upon evaporation of a concentrated chloroform solution, Dibanta-H produced unsolvated single crystals suitable for X-ray diffraction analysis.[30] In the solid state, the triazole exists as the 2*H* tautomer and forms a unique hydrogen-bonded tetrad $(Dibanta\text{-}H)_4$ (Figure 2A, and C). The latter assembly is nearly planar, with approximate fourfold symmetry, and to the best of our knowledge, has no precedent among reported crystal structures of triazoles. In particular, it differs from rhomboid-shaped tetrads reported for certain 1*H*-triazoles,[31,32] and triads observed for some 2*H*-triazole esters.[33,34] $(Dibanta\text{-}H)_4$ is stabilized by a set of four NH···N hydrogen bonds and four weaker CH···N interactions (engaging hydrogens b′, cf. Figure 2A), resembling the guanine tetrad found in nucleic acid G-quadruplexes. The Dibanta tetrads are arranged in tilted stacks in the solid state (Figure 2C), with interplanar distances of about 3.49–3.55 Å indicative of efficient π-stacking interactions.

In contrast to Dibanta-H, the unsubstituted reference system Anta-H was found to form triads $(Anta\text{-}H)_3$ in the solid state (Figure 2B and D). In these assemblies, which are visibly distorted from planarity, the triazoles also exist as 2*H* tautomers, and the H-bonded distances are less uniform than in the Dibanta tetrad. Specifically, the N···N distances are 2.81–2.91 Å in $(Anta\text{-}H)_3$ versus 2.84–2.88 Å in $(Dibanta\text{-}H)_4$. The Anta triads form π-stacks with a smaller interplanar distance of 3.41 Å, and a smaller offset relative to the stacking direction. These features are apparently consistent with the lack of bulky substitution on the Anta triazoles. In the Dibanta-H crystal, the larger offset in the stack enables interdigitation of *tert*-butyl groups between consecutive tetrads, but decreases the area of π overlap within the stack.

The ^1H NMR spectrum of Dibanta-H recorded in [D_6]acetone at 300 K (Figure S1 in the Supporting Information) showed a fully symmetric spectral pattern, with the triazole NH signal at 13.95 ppm. On lowering of the temperature to 190 K, the peak became narrower and was gradually shifted to 14.65 ppm, whereas the other resonances remained essentially unchanged.

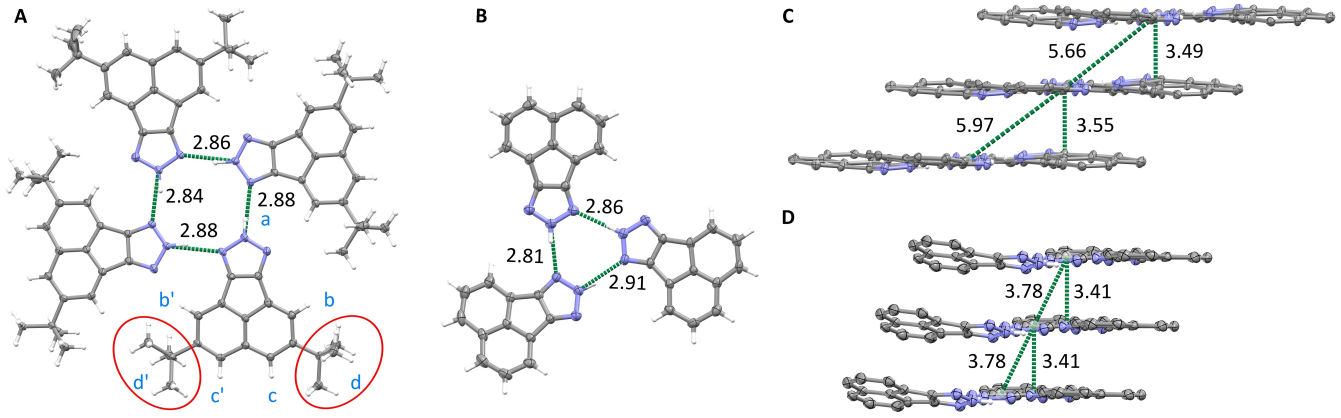

Figure 2. A) and B) Crystal structures of Dibanta-H and Anta-H and the formation of hydrogen-bonded tetrads and triads. Thermal ellipsoids are shown at the 50% probability level. C) and D) Stacking of tetrads and triads in the solid state. Distances between centroids (left) and mean planes of adjacent tetrads and triads (right) are given in Å. Peripheral hydrogens in (C) and (D) and *t*Bu groups in (C) are omitted for clarity.

These features indicate relatively strong H-bonded interactions of the triazole with the solvent, and suggest that Dibanta-H either exists as the 2*H* tautomer in solution, in accord with the XRD and DFT data, or that the tautomerization of the 1*H* tautomer is fast even at 190 K. In contrast, spectra recorded in [D_8]toluene showed remarkable changes upon cooling from 300 to 160 K. At 300 K, the NH signal was observed at 10.42 ppm, reflecting the less polar character of the solvent (Figure 3A). On lowering the temperature to 210 K, the NH peak was relocated to 12.98 ppm and became very broad. Below that temperature the spectrum became extremely broadened, but a relatively well resolved pattern could again be observed below 170 K. At 165 K, the spectrum contained two broad overlapping signals at about 16.5 ppm (a, Figure 3B), which could be assigned to NH protons on the basis of a D_2O exchange experiment (Figure 3C). The large downfield shift of these protons is consistent with strong hydrogen bonding, which in a nonpolar solvent can be reasonably ascribed to self-association of the triazoles.

The large number of signals in the 165 K spectrum indicates the predominance of two structurally similar species consisting of desymmetrized triazole subunits. The spectral pattern can be tentatively ascribed to the formation of two structurally similar aggregates, for example (Dibanta-H)$_4$, analogous to the tetrad observed in the crystal, and the corresponding triad (Dibanta-H)$_3$, similar to (Anta-H)$_3$. Alternatively, the two species might be thought to correspond to (Dibanta-H)$_4$ and its π-stacked dimer [(Dibanta-H)$_4$]$_2$. The latter aggregate would be analogous to discrete π-stacked dimers which are occasionally observable for extended aromatic surfaces in solution.[35] However, π stacking of aromatic cores typically produces significant upfield relocations of ^{1}H resonances, an effect that is not observed in the low temperature spectra of Dibanta-H. Thus the relative similarity of chemical shifts observed for the two species appears to be more consistent with the first hypothesis, that is, the coexistence of (Dibanta-H)$_3$ and (Dibanta-H)$_4$. A more detailed spectroscopic analysis using correlation and diffusion-ordered spectroscopic methods was not feasible because of extreme line broadening and unfavorable relaxation times. Supporting evidence for the formation of (Dibanta-H)$_3$ and (Dibanta-H)$_4$ could however be gained from DFT calculations (see below). Regardless of the actual identity of the two observed forms, the extreme broadening of ^{1}H NMR signals that occurs at temperatures lower than 165 K is likely caused by the onset of further, nonspecific aggregation.

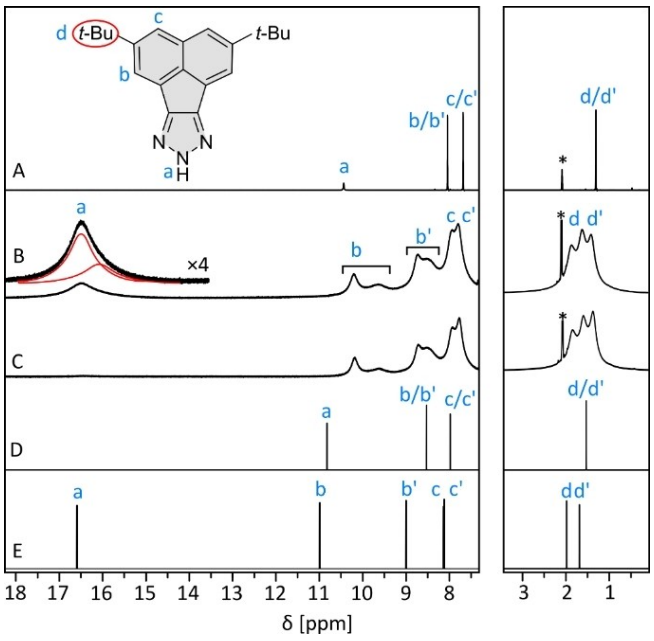

Figure 3. Experimental ^{1}H NMR spectra of Dibanta-H recorded in [D_8]toluene at A) 300 K, B) 165 K, and C) at 165 K after shaking with D_2O. The approximate positions of two overlapping NH peaks in (B) are indicated with red lines. GIAO chemical shifts for D) 2*H*-Dibanta-H and E) (2*H*-Dibanta-H)$_4$ (PCM(toluene)/ωB97XD/6-31G(d,p) level of theory).

Tautomerism and self-assembly thermodynamics of Anta-H and Dibanta-H were investigated using DFT calculations (Table 1). At the PCM(toluene)/ωB97XD/6-31G(d,p) level of theory, the 2*H* tautomers of Anta-H and Dibanta-H are more stable than the corresponding 1*H* tautomers by $\Delta G^{298} = 4.77$ and 4.75 kcal mol^{-1}, respectively, in line with the preference observed in the crystals. The greater stability of the 2H tautomer in these triazoles may be partly caused by the fused five-membered ring, which likely affects the bond lengths and valence angles within the triazole moiety in a way that promotes protonation on N2. The formation of the (2*H*-Dibanta-H)$_4$ tetrad is predicted to produce a free energy gain of −3.35 kcal mol^{-1} per monomer unit. In the optimized geometry, the assembly adopts a puckered shape, indicating that the tetrad is quite flexible and that π stacking may contribute to its near complete planarization in the crystal. The corresponding triad (2*H*-Dibanta-H)$_3$ is less stabilized (−1.61 kcal mol^{-1} per monomer), whereas an opposite preference is predicted for Anta-H, correlating with the crystal structure data. The greater stabilization of the (2*H*-Dibanta-H)$_4$ tetrad may be ascribed to dispersive interactions involving the bulky *tert*-butyl groups, which are largely absent in the triad.

GIAO/PCM(toluene)/ωB97XD/6-31G(d,p) simulations provide further support for the proposed assembly in solution. In particular, chemical shifts calculated for the monomeric 2*H*-Dibanta-H are in good agreement with the room temperature ^{1}H NMR spectrum, thus implying that the triazole remains mostly monomeric at this temperature (Figure 3D). In particular, the NH shift at 10.81 ppm is similar to that observed at room

Table 1. Relative energies of Anta-H and Dibanta-H monomers and their corresponding cyclic oligomers.

	ΔG^{298} [kcal mol^{-1}][a,b] **X** = Dibanta	**X** = Anta
2*H*-**X**-H	0.00	0.00
1*H*-**X**-H	4.75	4.77
(2*H*-**X**-H)$_3$	−1.61	−1.55
(1*H*-**X**-H)$_3$	0.96	1.11
(2*H*-**X**-H)$_4$	−3.35	−1.27
(1*H*-**X**-H)$_4$	−0.67	0.82

[a] PCM(toluene)/ωB97XD/6-31G(d,p). [b] Energy per monomer unit relative to the lowest energy tautomer.

temperature, in line with the assumed absence of strong hydrogen bonding. In comparison, GIAO data obtained for (2*H*-Dibanta-H)$_4$ (Figure 3E) show markedly differentiated shifts of protons b and b′, with a characteristic downfield value of b, which is reflected in the experimental data. The calculated shift of the NH signal of 16.59 ppm demonstrates the effect of hydrogen bonding and is also in quantitative agreement with the low-temperature spectrum.

Molecular structures of $[Zn_5Cl_4(Dibanta)_6]$ and $[Zn_5Cl_4(Cybta)_6]$ were confirmed by single-crystal X-ray diffraction analysis and shown to contain the Kuratowski-type pentanuclear coordination unit (Figure 4). The five Zn^{2+} ions form a body-centered tetrahedron, with an octahedrally coordinated ion at the center surrounded by four tetrahedrally coordinated ions at the vertices. In each case, six triazolate ligands span the edges of the tetrahedron, and the structure is completed by four apical chloride ligands. In $[Zn_5Cl_4(Dibanta)_6]$, the chlorides form close van der Waals contacts with the surrounding CH bonds of acenaphthylene, providing for a highly compact 3D arrangement. The structure does not however appear to be sterically congested, since the Zn–N distances are typical (2.00–2.03 Å and 2.16–2.20 Å, for tetrahedral and octahedral centers, respectively).

An important consequence of π-extension of triazole ligands in the above Kuratowski complexes is the formation of internal molecular free volume (IMFV).[37,38] This volume is partitioned into four prismatic voids, one at each face of the Kuratowski tetrahedron. The total IMFV for $[Zn_5Cl_4(Dibanta)_6]$ can be estimated conservatively as approximately 250 Å^3, using a simple geometrical analysis (see the Supporting Information). In the crystals of $[Zn_5Cl_4(Dibanta)_6]$ and $[Zn_5Cl_4(Cybta)_6]$, the IMFV cavities are occupied by solvent molecules (DMF/2,6-lutidine and chloroform, respectively). Pore volumes, estimated using contact surface calculations[36,39] (Figure 4, Table S13), were found to be larger in the crystals of $[Zn_5Cl_4(Dibanta)_6]$ (32–34% vs. ca. 22% for $[Zn_5Cl_4(Cybta)_6]$). These values are smaller than the upper bounds estimated from van der Waals molecular volumes of these two complexes (52 and 44%, respectively). Nitrogen absorption data obtained for solid $[Zn_5Cl_4(Dibanta)_6]$ yielded an estimated BET surface area of 332.5 $m^2 g^{-1}$, with a pore width of 15 Å. In contrast, the surface area of solid $[Zn_5Cl_4(Cybta)_6]$ was significantly lower (10.3 $m^2 g^{-1}$), in line with the less extended structure of the Cybta-H ligand (cf. Figures S4 and S5).

The influence of the extended π-conjugated system on the photophysical characteristics of Kuratowski complexes $[Zn_5Cl_4(Cybta)_6]$ and $[Zn_5Cl_4(Dibanta)_6]$ was investigated using UV-vis absorption spectroscopy, steady-state fluorescence spectroscopy and fluorescence life-time measurements (Figures 5 and S6–S46, Table 2). Cybta-H and Dibanta-H, as well as their Kuratowski complexes, show well-defined absorption bands and linear concentration dependence of absorbance in dilute chloroform solutions. In particular, solutions of Cybta-H and its Kuratowski complex show similar absorption bands (λ_{max}^{abs} = 290 nm), and nearly identical fluorescence emission (λ_{max}^{abs} = 357 nm). The excitation and emission behavior of these two compounds is also similar in the solid state. The absorption spectrum of Dibanta-H contains several bands reaching up to about 400 nm. This red shift relative to the absorption of Cybta-H is attributed to the more extended π system of Dibanta-H. The emission of the latter triazole has a maximum at 440 nm, yielding observable blue fluorescence with a quantum yield of

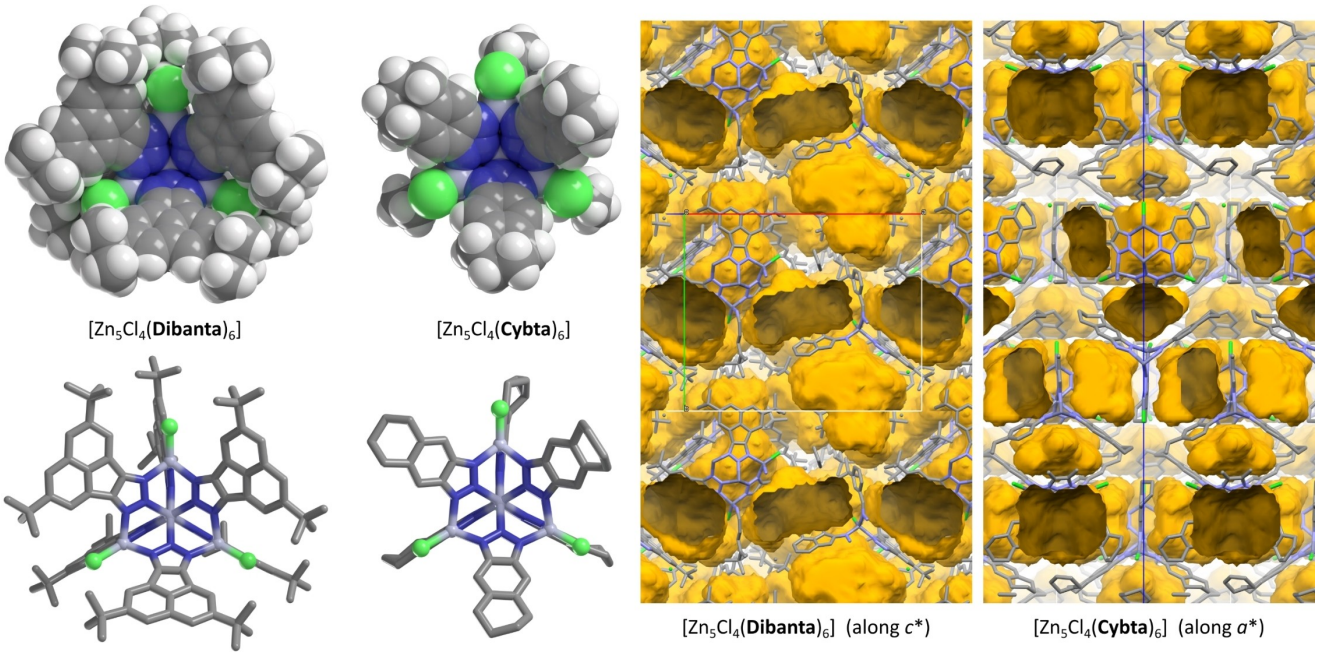

Figure 4. Left: Molecular structures of $[Zn_5Cl_4(Dibanta)_6]$ and $[Zn_5Cl_4(Cybta)_6]$ obtained from an X-ray diffraction analyses. Solvent molecules and hydrogen atoms (in stick models) are removed for clarity. Right: Contact surfaces (1.2 Å probe radius, orange),[36] calculated for the crystal structures with solvent molecules removed from the model. The corresponding void volumes are 34.1 and 21.9% for $[Zn_5Cl_4(Dibanta)_6]$ and $[Zn_5Cl_4(Cybta)_6]$ respectively.

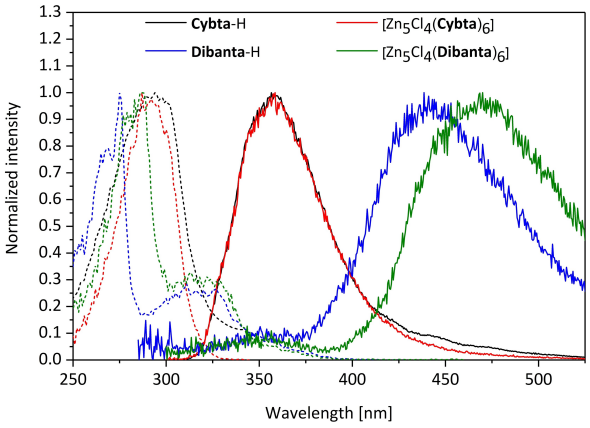

Figure 5. Excitation (-----) and emission (——) spectra of Cybta-H and Dibanta-H and their Kuratowski complexes measured in chloroform.

Table 2. Absorption and emission properties of triazoles and their complexes.

Compd	Solvent	λ_{max}^{abs} [nm]	λ_{max}^{em} [nm]	QY[a] [%]	τ_1 (τ_2) [ns]
Cybta-H	$CHCl_3$	290	357	11.39	0.24 (3.59)
	solid	290	445	[b]	0.55 (18.83)
$[Zn_5Cl_4(Cybta)_6]$	$CHCl_3$	290	357	25.12	0.18 (3.63)
	solid	325	448	[b]	1.28 (19.83)
Dibanta-H	$CHCl_3$	275	440	4.79	14.22
	solid	275	440	[b]	3.58 (25.92)
$[Zn_5Cl_4(Dibanta)_6]$	$CHCl_3$	288	470	2.56	10.16
	solid	330	465	[b]	2.56 (20.83)

[a] Fluorescence quantum yield determined according to the relative method of Williams et al.[40] [b] Not measured.

around 5 %. A further red shift (λ_{max}^{abs} = 470 nm) and a diminished quantum yield were determined for $[Zn_5Cl_4(Dibanta)_6]$.

In solution, the fluorescence decay of Cybta-H and $[Zn_5Cl_4(Cybta)_6]$ is biexponential with a dominant contribution of the τ_2 component of about 3.7 ns (Table 2). The fluorescence lifetimes of Dibanta-H and $[Zn_5Cl_4(Dibanta)_6]$ are longer (ca. 14 and 10 ns, respectively), apparently correlating with the enlargement of the π-conjugated chromophore. All compounds show longer fluorescence lifetimes in the solid state than in solution and the behavior is biexponential in all cases. These features are likely caused by intermolecular interactions in the solid state, including hydrogen-bonded self-assembly of higher aggregates.

In summary, three easy-to-make aromatic triazoles, the small Cybta-H and the π-extended acenaphthylene-fused Dibanta-H and Anta-H, were synthesized and characterized. In particular, Dibanta-H is shown to be a useful motif for the assembly of two- and three-dimensional molecular architectures. The formation of stacked hydrogen-bonded tetrads $(Dibanta\text{-}H)_4$, reminiscent of G-quadruplexes, has no precedent in triazole chemistry and might possibly be employed as a square planar tetravalent junction in discotic liquid crystals or complex molecular assemblies. In spite of its steric bulk, Dibanta-H forms a pentanuclear Kuratowski complex with Zn^{II}, displaying large intramolecular free volumes and enhanced porosity in the solid state. This result suggests that Kuratowski-type secondary building units based on similar π-extended triazoles might provide access to MOFs analogous to, for example, MFU-4 and CFA-1, combining intrinsically high porosity with electronic characteristics and tunable photophysical characteristics inherited from the π system of the triazole ligands. Efforts to explore these possibilities are currently ongoing in our laboratories.

Acknowledgements

Financial support was kindly provided as part of the Polish-German BEETHOVEN CLASSIC program funded jointly by the National Science Center of Poland (UMO-2018/31/G/ST5/01813, to M.S.) and the German Science Foundation (DFG, VO 829/14-1, to D.V.). Financial support from the Foundation for Polish Science (TEAM POIR.04.04.00-00-5BF1/17-00 M.S.) is gratefully acknowledged. Quantum chemical calculations were performed in the Wrocław Center for Networking and Supercomputing. Open Access funding enabled and organized by Projekt DEAL.

Conflict of Interest

The authors declare no conflict of interest.

Keywords: chromophores · computational chemistry · coordination chemistry · NMR spectroscopy · triazoles

[1] M. Stępień, E. Gońka, M. Żyła, N. Sprutta, *Chem. Rev.* **2017**, *117*, 3479–3716.
[2] T. Sarma, P. K. Panda, *Chem. Rev.* **2017**, *117*, 2785–2838.
[3] T. D. Lash, P. Chandrasekar, *J. Am. Chem. Soc.* **1996**, *118*, 8767–8768.
[4] T. Okujima, C. Ando, J. Mack, S. Mori, I. Hisaki, T. Nakae, H. Yamada, K. Ohara, N. Kobayashi, H. Uno, *Chem. Eur. J.* **2013**, *19*, 13970–13978.
[5] H. Zhylitskaya, J. Cybińska, P. Chmielewski, T. Lis, M. Stępień, *J. Am. Chem. Soc.* **2016**, *138*, 11390–11398.
[6] M. Żyła-Karwowska, H. Zhylitskaya, J. Cybińska, T. Lis, P. J. Chmielewski, M. Stępień, *Angew. Chem. Int. Ed.* **2016**, *55*, 14658–14662. *Angew. Chem.* **2016**, *128*, 14878–14882.
[7] M. Żyła-Karwowska, L. Moshniaha, Y. Hong, H. Zhylitskaya, J. Cybińska, P. J. Chmielewski, T. Lis, D. Kim, M. Stępień, *Chem. Eur. J.* **2018**, *24*, 7525–7530.
[8] M. Navakouski, H. Zhylitskaya, P. J. Chmielewski, T. Lis, J. Cybińska, M. Stępień, *Angew. Chem. Int. Ed.* **2019**, *58*, 4929–4933. *Angew. Chem.* **2019**, *131*, 4983–4987.
[9] L. Moshniaha, M. Żyła-Karwowska, P. J. Chmielewski, T. Lis, J. Cybińska, E. Gońka, J. Oschwald, T. Drewello, S. M. Rivero, J. Casado, M. Stępień, *J. Am. Chem. Soc.* **2020**, *142*, 3626–3635.
[10] S. Kumar, Y. K. Maurya, S. Kang, P. Chmielewski, T. Lis, J. Cybińska, D. Kim, M. Stępień, *Org. Lett.* **2020**, *22*, 7202–7207.
[11] T. Tu, W. Fang, J. Jiang, *Chem. Commun.* **2011**, *47*, 12358–12360.
[12] A. Prades, E. Peris, M. Alcarazo, *Organometallics* **2012**, *31*, 4623–4626.
[13] Y. Cai, X.-T. Yang, S.-Q. Zhang, F. Li, Y.-Q. Li, L.-X. Ruan, X. Hong, S.-L. Shi, *Angew. Chem. Int. Ed.* **2018**, *57*, 1376–1380. *Angew. Chem.* **2018**, *130*, 1390–1394.
[14] J. Diesel, A. M. Finogenova, N. Cramer, *J. Am. Chem. Soc.* **2018**, *140*, 4489–4493.
[15] J. H. Marshall, *Inorg. Chem.* **1978**, *17*, 3711–3713.

[16] V. L. Himes, A. D. Mighell, A. R. Siedle, *J. Am. Chem. Soc.* **1981**, *103*, 211–212.
[17] G. F. Kokoszka, J. Baranowski, C. Goldstein, J. Orsini, A. D. Mighell, V. L. Himes, A. R. Siedle, *J. Am. Chem. Soc.* **1983**, *105*, 5627–5633.
[18] C. Kuratowski, *Fundam. Math.* **1930**, *15*, 271–283.
[19] S. Biswas, M. Tonigold, M. Speldrich, P. Kögerler, M. Weil, D. Volkmer, *Inorg. Chem.* **2010**, *49*, 7424–7434.
[20] Y.-L. Bai, J. Tao, R.-B. Huang, L.-S. Zheng, *Angew. Chem. Int. Ed.* **2008**, *47*, 5344–5347. *Angew. Chem.* **2008**, *120*, 5424–5427.
[21] X.-L. Wang, C. Qin, S.-X. Wu, K.-Z. Shao, Y.-Q. Lan, S. Wang, D.-X. Zhu, Z.-M. Su, E.-B. Wang, *Angew. Chem. Int. Ed.* **2009**, *48*, 5291–5295. *Angew. Chem.* **2009**, *121*, 5395–5399.
[22] S. Biswas, M. Grzywa, H. P. Nayek, S. Dehnen, I. Senkovska, S. Kaskel, D. Volkmer, *Dalton Trans.* **2009**, *0*, 6487–6495.
[23] P. Schmieder, D. Denysenko, M. Grzywa, B. Baumgärtner, I. Senkovska, S. Kaskel, G. Sastre, L. van Wüllen, D. Volkmer, *Dalton Trans.* **2013**, *42*, 10786–10797.
[24] P. Schmieder, M. Grzywa, D. Denysenko, M. Hambach, D. Volkmer, *Dalton Trans.* **2015**, *44*, 13060–13070.
[25] P. Schmieder, D. Denysenko, M. Grzywa, O. Magdysyuk, D. Volkmer, *Dalton Trans.* **2016**, *45*, 13853–13862.
[26] A. G. Anderson, R. G. Anderson, *J. Am. Chem. Soc.* **1955**, *77*, 6610–6611.
[27] A. W. Amick, K. S. Griswold, L. T. Scott, *Can. J. Chem.* **2006**, *84*, 1268–1272.
[28] T. W. Werner, S. Reschke, H. Bunzen, H.-A. K. von Nidda, J. Deisenhofer, A. Loidl, D. Volkmer, *Inorg. Chem.* **2016**, *55*, 1053–1060.
[29] H. Bunzen, M. Grzywa, A. Kalytta-Mewes, D. Volkmer, *Dalton Trans.* **2017**, *46*, 2618–2625.
[30] Deposition Numbers 2104029 (for Anta-H), 2067995 (for Dibanta-H), 2108787 (for $[Zn_5Cl_4(Cybta)_6]$) and 2109385 (for $[Zn_5Cl_4(Dibanta)_6]$) contain the supplementary crystallographic data for this paper. These data are provided free of charge by the joint Cambridge Crystallographic Data Centre and Fachinformationszentrum Karlsruhe Access Structures service.
[31] D. V. Partyka, J. B. Updegraff, M. Zeller, A. D. Hunter, T. G. Gray, *Organometallics* **2007**, *26*, 183–186.
[32] C. J. Zeman, Y.-H. Shen, J. K. Heller, K. A. Abboud, K. S. Schanze, A. S. Veige, *J. Am. Chem. Soc.* **2020**, *142*, 8331–8341.
[33] Y. Gao, Y. Lam, *Org. Lett.* **2006**, *8*, 3283–3285.
[34] Y. Wang, P. Yu, Q. Ren, F. Jia, Y. Chen, A. Wu, *J. Org. Chem.* **2020**, *85*, 2688–2696.
[35] D. Myśliwiec, B. Donnio, P. J. Chmielewski, B. Heinrich, M. Stępień, *J. Am. Chem. Soc.* **2012**, *134*, 4822–4833.
[36] C. F. Macrae, I. Sovago, S. J. Cottrell, P. T. A. Galek, P. McCabe, E. Pidcock, M. Platings, G. P. Shields, J. S. Stevens, M. Towler, P. A. Wood, *J. Appl. Crystallogr.* **2020**, *53*, 226–235.
[37] T. M. Long, T. M. Swager, *Adv. Mater.* **2001**, *13*, 601–604.
[38] N. T. Tsui, A. J. Paraskos, L. Torun, T. M. Swager, E. L. Thomas, *Macromolecules* **2006**, *39*, 3350–3358.
[39] L. Sarkisov, R. Bueno-Perez, M. Sutharson, D. Fairen-Jimenez, *Chem. Mater.* **2020**, *32*, 9849–9867.
[40] A. T. R. Williams, S. A. Winfield, J. N. Miller, *Analyst* **1983**, *108*, 1067–1071.

Manuscript received: September 23, 2021
Accepted manuscript online: October 28, 2021
Version of record online: December 2, 2021